Available online at www.sciencedirect.com
ScienceDirect
Journal of Nuclear Materials 372 (2008) 400–404
journal of nuclear materials
www.elsevier.com/locate/jnucmat

EBSD for microstructure and property characterization of the SiC-coating in TRISO fuel particles

L. Tan [a,*], T.R. Allen [a], J.D. Hunn [b], J.H. Miller [b]

[a] University of Wisconsin-Madison, Madison, WI 53706, USA
[b] Oak Ridge National Laboratory, Oak Ridge, TN 37831, USA

Received 11 December 2006; accepted 12 April 2007

Abstract

Tristructural-isotropic (TRISO)-coated particle fuel is being developed for use in the Next Generation Nuclear Plant. The reliable and precise characterization of the microstructure and properties of the SiC layer in the TRISO particle is essential for optimizing processing parameters to ensure reproducibility and performance of the coatings. Electron backscatter diffraction (EBSD) is a time-efficient analytical tool for obtaining a wealth of information on the SiC layer. In this study, we report the application of EBSD to the analysis of the SiC layer in a TRISO particle. The SiC layer identified as 3C–SiC with an average elastic stiffness of ~402 GPa was mainly composed of random boundaries with a small fraction of low-Σ CSLBs. A few large grains, which were generally associated with local strains and tended to be columnar with the long axis oriented approximately along the TRISO particle radial direction, were observed in the SiC layer with an increased population from the IPyC–SiC to the SiC–OPyC interfaces.

PACS: 81.40.−z; 07.10.Pz; 62.20.Dc; 61.72.Mm

1. Introduction

Tristructural-isotropic (TRISO)-coated particle fuel is currently used in high temperature gas-cooled reactors and will be the fuel for the Generation IV Very High Temperature Reactor (VHTR). Although this fuel type has been around for many years, fabrication in the United States is starting afresh, and with this renewed impetus, understanding the relationship between fuel fabrication and performance is critical to mitigating technical risk and uncertainty.

TRISO-coated fuels are typically composed of a heavy metal (e.g., uranium, plutonium, thorium, etc.) oxide or mixed oxide/carbide fuel kernel coated with four layers of three isotropic materials. The four layers are a porous carbon layer (buffer), followed by three sequential layers: a dense inner pyrolytic carbon layer (IPyC), a silicon carbide layer (SiC), and a dense outer pyrolytic carbon layer (OPyC). The role of the SiC layer is critical since it not only provides the TRISO particle with structural integrity but also retains fission products at elevated temperatures. In addition to SiC, other carbides such as ZrC with competitive/superior performance are being developed for TRISO coatings. Due to the critical role of the SiC layer, this layer and its interfaces with the IPyC and OPyC layers require reliable characterization for optimizing processing parameters to ensure performance and reproducibility of the coatings. Many reported results are mostly based on scanning electron microscopy (SEM) characterization, which only provides morphological information and, in some cases, grain size distributions. Such information is not sufficient for relating the detailed grain structure of the SiC layer to the important role in fission product retention [1]. Helary et al. [2] recently demonstrated that electron backscatter diffraction (EBSD) can be used for microstructure analysis of the SiC layer, such as identifying grain

* Corresponding author. Tel.: +1 608 262 7476; fax: +1 608 263 7451.
E-mail address: lizhentan@wisc.edu (L. Tan).

0022-3115/$ - see front matter © 2007 Elsevier B.V. All rights reserved.
doi:10.1016/j.jnucmat.2007.04.048

morphology, orientation, and special boundaries like Σ3, obtaining quantitative data on grain elongation, and determining texture. This paper attempts to fully exploit the capability of EBSD for microstructure and property analysis of SiC in TRISO particles.

2. Experiment

A TRISO coating was applied at the Oak Ridge National Laboratory (ORNL) to ~530 μm diameter yttria-stabilized ZrO_2 kernels by chemical vapor deposition (CVD) using an uninterrupted process in a 50 mm diameter fluidized bed furnace with a single inlet conical distributer [3]. Table 1 shows the key coating parameters. The listed deposition temperatures are the initial average particle bed temperatures. Bed temperature was controlled by a pyrometer focused on the outside wall of the coating chamber. IPyC and OPyC were deposited using a 1:1 mix of acetylene and propylene in argon. SiC was deposited using a 1:1 mixture of argon and hydrogen for fluidization with methyl trichlorosilane (MTS) carried to the furnace by bubbling hydrogen through liquid MTS. Coating gas fraction (CGF) is the fraction of coating gas in the total flow of gas used to fluidize the particles. The density of the SiC and OPyC layers was determined using a liquid gradient density column. The density of the buffer and IPyC layers could not be measured in the TRISO-coated particles but is typically around 1.2 g/cm^3 for buffer and 1.9 g/cm^3 for IPyC deposited under these conditions.

Cross-sections of the TRISO particles were prepared for SEM and EBSD analysis. To obtain good quality EBSD patterns, the cross-section samples were polished with SiC abrasive paper to 1200 grit followed by diamond paste, alpha alumina, and colloidal silica solutions in sequence. The EBSD investigation was performed on a LEO 1530 FEG-SEM incorporated with an EDAX's TSL orientation imaging microscopy (OIM) system MSC2200. The SEM was operated at 20 kV, and the automatic EBSD area scan was performed using a hexagonal grid with a step size of 0.1 μm and took ~2 h.

3. Results and discussion

An overview of the cross-section of a TRISO particle is shown in Fig. 1(a), which indicates that the particle and the SiC layer are not ideal spheres. The mean diameter aspect ratio (D_{max}/D_{min}) of the particles, based on a shadow image analysis of 1368 particles, is 1.045 ± 0.016 [3]. The backscatter electron image (BEI), shown in Fig. 1(b), zoomed in from the selected area marked in (a) clearly shows the coating layer structure. The buffer layer is porous compared to the other layers. Some polishing residues were trapped in this layer in a morphology of white sparsely distributed spots. EBSD analysis was performed on a select area marked in Fig. 1(b). The EBSD scanning map is shown in Fig. 1(c) indicating the phase distribution and grain boundaries. The SiC layer was identified by EBSD to consist of 3C–SiC (face-centered cubic, fcc). In addition to the fcc structure, SiC has other polytypes such as α-SiC in hexagonal structure. EBSD could easily differentiate the phases due to their significantly different crystallography which results in different Kikuchi bands in orientation and width. 3C–SiC has been observed to be a predominant polytype for CVD-fabricated SiC [2,4]. Helary et al. [5],

Table 1
Deposition conditions for TRISO coating

	Buffer	IPyC	SiC	OPyC
Deposition temperature (°C)	1256	1256	1410	1256
Coating gas	C_2H_2	$C_2H_2 + C_3H_6$ (1:1)	MTS in H	$C_2H_2 + C_3H_6$ (1:1)
Additional fluidization gas	Ar	Ar	Ar + H (1:1)	Ar
Coating gas fraction	0.6	0.3	0.014	0.3
Average deposition rate (μm/min)	17	4.6	0.2	4.5
Layer thickness (μm)	85 ± 4	41 ± 3	31 ± 1	36 ± 2
Layer density (g/cm^3)	–	–	3.205 ± 0.001	2.012 ± 0.002

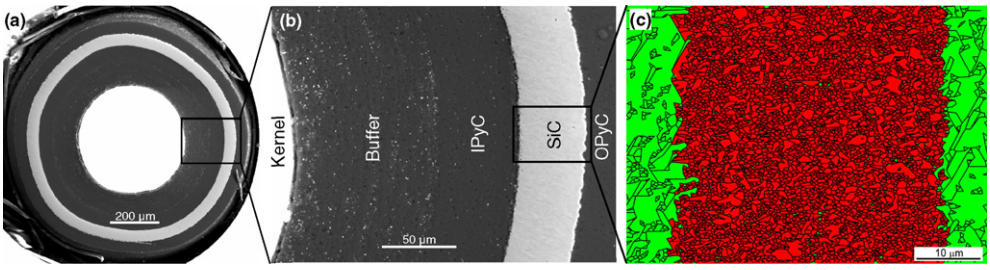

Fig. 1. SEM–EBSD analyses of a TRISO particle prepared by ORNL, which is composed of a yttria stabilized zirconia kernel covered by buffer, IPyC, SiC, and OPyC layers. (a) A low-magnification cross-section SEM image (backscatter electron image – BEI). (b) A medium-magnification BEI of a selected area marked in (a). (c) A high-magnification EBSD map of a selected region marked in (b), which illustrates grain boundaries and phase distribution.

using high resolution transmission electron microscopy, reported the observation of a very small amount of α-SiC with a size of <50 nm distributed in 3C–SiC matrix. However, this small size α-SiC, if present in this study, is too small to be resolved by EBSD.

A high-magnification BEI of the SiC layer between the IPyC and OPyC layers is shown in Fig. 2. The image contrast illustrates smaller grains close to the IPyC layer with some large grains formed close to the OPyC layer. Different interface morphology is clearly shown in Fig. 2. The IPyC–SiC interface shows extensive interfacial stitching with a thickness of ~2 μm, while the SiC–OPyC interface is well defined and without discernable interfacial stitching. Similar interface morphologies were also noticeable by EBSD analysis as shown in Fig. 1(c). These different interface morphologies are a result of the difference in the open porosity of the IPyC and SiC layers. The relatively high open porosity of the IPyC surface (1–1.5 mL/m^2) allows the SiC to infiltrate several micrometers into the IPyC. In contrast, stitching at the SiC/OPyC interface is minimal due to nearly zero open porosity at the SiC surface.

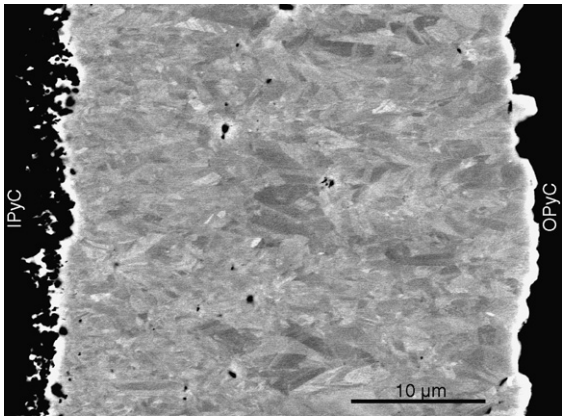

Fig. 2. SEM image (BEI) of the SiC layer between the IPyC and OPyC layers.

Grain size and grain boundary character distribution (GBCD) of the SiC layer were analyzed by EBSD and the results are shown in Fig. 3. GBCD was evaluated by the Brandon criterion [6] defining the allowable deviation from the exact orientation relationship. Most grains are submicron in size. The grain morphology of the SiC layer is shown in the inset of Fig. 3(a) with Σ3 boundaries highlighted in white. Because of the small stacking fault energy of the 3C–SiC [7], the twin boundaries (Σ3) were generally formed in association with large columnar grains grown during deposition. More large columnar grains were observed close to the OPyC layer. This may be due to less nucleation of new grains and less constraint by neighboring grains as the deposition progressed. The GBCD result as shown in the inset of Fig. 3(b) indicates that more than half of the grain boundaries are random boundaries (large-angle boundaries except for the low-Σ coincidence site lattice boundaries (CSLBs) with $3 \leqslant \Sigma \leqslant 29$). Low-Σ CSLBs only make up ~12% of the GBCD. The twin (Σ3) and twin variant (Σ9 and Σ27) boundaries are the dominant population of low-Σ CSLBs, which is consistent with the universal features of GBCD in face-centered cubic polycrystalline systems [8]. The observed low-Σ CSLBs are not expected to be detrimental to the performance of the SiC. In fact, low-Σ CSLBs, especially Σ3 boundaries, are generally beneficial for retarding diffusion and improving mechanical properties due to their low energies [9]. However, most of the low-Σ CSLBs are isolated by random boundaries. Thus, the small fraction of low-Σ CSLBs in the SiC layer is not expected to provide significant performance enhancement.

The corresponding (1 1 1) pole figure of the SiC layer is shown in Fig. 4, indicating a weak texture. The areas of maximum texture intensity in Fig. 4 were associated with most of the larger grains, which indicates that these grains were most often oriented in a direction nearly normal to the growth surface (ND) (i.e., parallel to the deposition direction). This is because extended grain growth in the

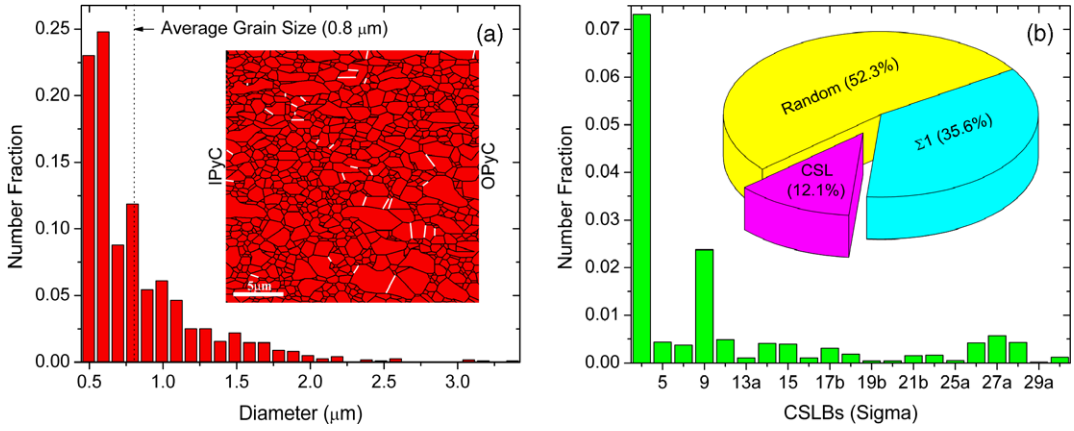

Fig. 3. Grain and grain boundary analyses of the SiC (3C) layer. (a) Grain size distribution of the SiC layer as shown in the inset with Σ3 boundaries highlighted in white. (b) Population of the low-Σ CSLBs ($3 \leqslant \Sigma \leqslant 29$) with the overall grain boundary character distribution (GBCD: Σ1, low-Σ CSL, and random boundaries) as the inset.

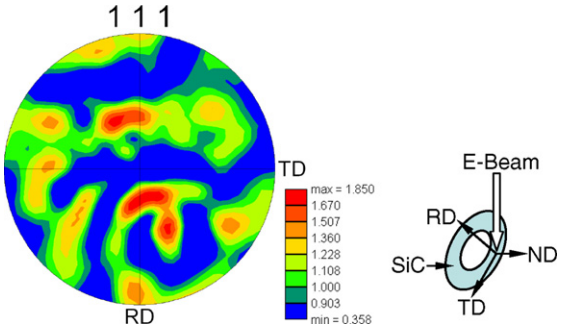

Fig. 4. Corresponding (1 1 1) pole figure for the SiC layer. A schematic illustration of a cross-section sample shows the orientations of ND (the center of the pole figure, the direction normal to the TRISO particle surface paralleling to the deposition direction), TD (tangent to the surface of the particle in the plane of the cross-section), and RD (normal to the plane of the cross-section).

SiC layer was restrained by the surrounding grains causing the deposition direction to become the preferred direction for grain growth. As discussed in Ref. [2], (1 1 1) is the most energetically favored growth direction for 3C–SiC. Grains with (1 1 1) not parallel to ND are limited in size because of the constraint from neighboring grains. In contrast, grains with a (1 1 1) axis oriented in the growth direction are only constrained in the growth plane, and can grow into long columns in the (1 1 1) direction. In Fig. 4, it can be seen that the growth direction deviated somewhat from the ND, which may be because deposition in this temperature range tended to randomize the growth [10]. A similar result was also observed in Ref. [2].

Local strains developed in the SiC layer when cooled down from the deposition temperature as a result of the defects and local anisotropies in the material. Local strain distribution can be presented in EBSD maps in a number of different ways. Local average misorientation between each data point measurement and its neighbors, excluding any higher angle boundaries (>5°), was calculated as a

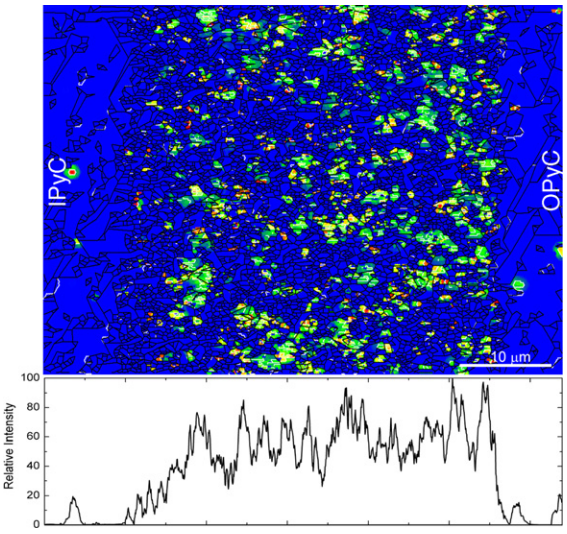

Fig. 5. Strain distribution represented by local misorientation map (0–5° average misorientation). The profile aligned below the map indicates the relative strain intensity integrated along the vertical direction in the map.

means to qualitatively represent local strain variations. Fig. 5 shows a region of the SiC mapped in this way. Because deformed regions have a higher concentration of low-angle boundaries (e.g. 1–15° misorientation), they are also included in Fig. 5 as white lines to locate these strain zones. The low-angle boundaries overlapping with the local average misorientation indicates the consistency of these two presenting methods. The relative strain intensity integrated along the vertical direction in the average misorientation map (normal to the radial direction of the TRISO particle) is also shown in Fig. 5. The results of this analysis indicate that the strains increase with increasing particle radius and reach a maximum close to the SiC–OPyC interface. The strain zones are mostly associated with the (1 1 1)-textured large columnar grains.

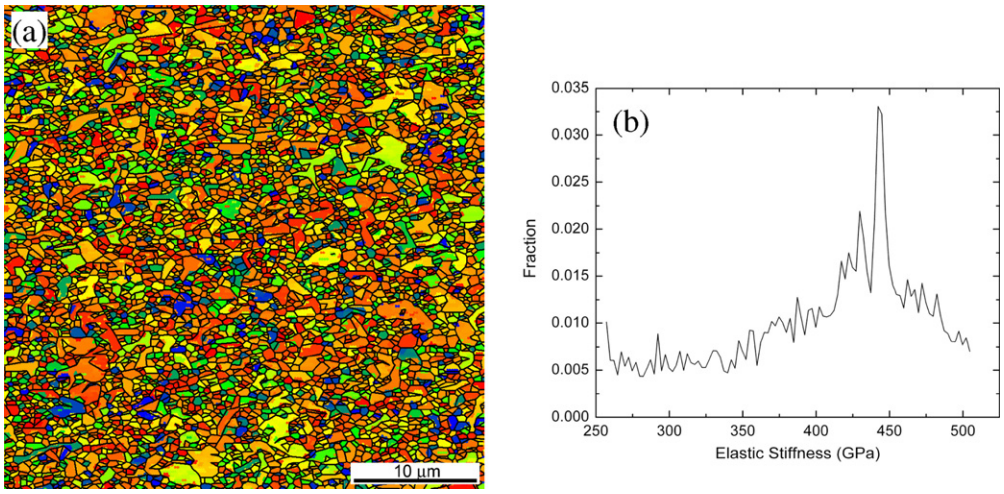

Fig. 6. (a) Elastic stiffness map of the SiC layer (256–506 GPa) calculated assuming uniaxial compression in a direction normal to the TRISO particle surface (parallel to the deposition direction). The IPyC–SiC and SiC–OPyC interfaces are on the left and right side of the figure, respectively. (b) Distribution of elastic stiffness of the SiC layer.

As a structural material for the TRISO particle, mechanical properties of the SiC layer are critical. Although the average elastic properties of polycrystalline materials are generally assumed to be isotropic, the elastic properties of single crystal material can be quite anisotropic. Based on the crystal orientation data from the EBSD analysis and the single crystal elastic constants of 3C–SiC from Ref. [11], the elastic stiffness of the SiC layer was calculated assuming the material experienced uniaxial compression normal to the TRISO particle surface (radial direction). The result shown in Fig. 6 indicates the variation in elastic stiffness due to differences in crystal orientation. The stiffness calculated with these assumptions is in a range of 256–506 GPa with an average of ~402 GPa, which is consistent with Ref. [12]. The presence of the regions with low stiffness as shown in Fig. 6(a) is not expected to be detrimental for the structural stability of the material due to their discrete and isolated distribution. The large columnar grains associated with the (1 1 1) texture and the local strains have two general levels of stiffness: ~380 GPa and ~440 GPa. The higher level of stiffness of the large grains shows up in the greatest fraction of stiffness as shown in Fig. 6(b). The higher stiffness coupled with local strain may result in higher local pressure or stress. This is consistent with the observation that columnar microstructures have higher residual stresses than equiaxed microstructures of 3C–SiC [13].

4. Conclusion

As an example of the capabilities of electron backscatter diffraction, the microstructure and associated properties of the SiC layer in a TRISO-coated particle were investigated. Different morphologies were observed at the interfaces of IPyC–SiC and SiC–OPyC. The SiC layer was identified to contain 3C–SiC. The grain boundaries in the SiC layer were mainly composed of random boundaries with a small fraction of low-Σ CSLBs. A few large grains were observed in the SiC layer, and the population increased when moving from the IPyC–SiC to the SiC–OPyC interfaces. The larger grain growth tended to be columnar with the long axis oriented approximately along the TRISO particle radial direction. Local strain zones were generally associated with the large grains and were found primarily close to the SiC–OPyC interface. The calculated elastic stiffness of the SiC layer was consistent with the literature reported value. The presence of regions with low elastic stiffness is not expected to be detrimental to the structural stability of the SiC layer due to their discrete distribution. This study indicates that EBSD is a time-efficient and versatile tool applicable for evaluating the microstructure and properties of advanced materials like TRISO fuel particles.

Acknowledgements

The work was supported under contract No. DE-FC07-06ID14740 (sponsored by the Department of Energy Office of Nuclear Energy, Science, and Technology NERI program (project 06-007)) and No. DE-ACO5-00OR22725 (sponsored by the DOE Office of Nuclear Energy, Science, and Technology's Advanced Gas Reactor Program and Oak Ridge National Laboratory, managed by UT-Battelle, LLC).

References

[1] D.A. Petti, J. Buongiorno, J.T. Maki, G.K. Miller, R.R. Hobbins, in: Proceedings of the Conference on High Temperature Reactors (HTR-2002), Petten, NL, 22–24 April, 2002.
[2] D. Helary, O. Dugne, X. Bourrat, P.H. Jouneau, F. Cellier, J. Nucl. Mater. 350 (2006) 332.
[3] A.K. Kercher, J.D. Hunn, Report ORNL/TM-2005/540, June 2005.
[4] K.A. Appiah, Z.L. Wang, W.J. Lackey, Thin Solid Films 371 (2000) 114.
[5] D. Helary, X. Bourrat, O. Dugne, G. Maveyraud, M. Perez, P. Guillermier, in: The 2nd International Topical Meeting on High Temperature Reactor Technology, Beijing, China, 22–24 September, 2004.
[6] D.G. Brandon, Acta Metall. 14 (1966) 1479.
[7] H. Iwata, Mater. Sci. Forum 389–393 (2002) 439.
[8] C.A. Schuh, M. Kumar, W.E. King, J. Mater. Sci. 40 (2005) 847.
[9] V. Randle, The Role of the Coincidence Site Lattice in Grain Boundary Engineering, The Institute of Materials, London, 1996.
[10] E. Hurtos, J. Rodriguez-Viejo, J. Appl. Phys. 87 (2000) 1748.
[11] K. Karch, P. Pavone, W. Windl, O. Schutt, D. Strauch, Phys. Rev. B 50 (1994) 17054.
[12] L. Tong, M. Mehregany, L.G. Matus, Appl. Phys. Lett. 60 (1992) 2992.
[13] S. Roy, C. Zorman, M. Mehregany, R. DeAnna, C. Deeb, J. Appl. Phys. 99 (2006) 044108.